Int. J. Heat Mass Transfer. Vol. 28, No. 4, pp. 741–752, 1985
Printed in Great Britain

0017–9310/85 $3.00 + 0.00

Natural convection from variously oriented cubes and from other bodies of unity aspect ratio

E. M. SPARROW and A. J. STRETTON
Department of Mechanical Engineering, University of Minnesota, Minneapolis, MN 55455, U.S.A.

(*Received* 24 *August* 1984 *and in final form* 31 *October* 1984)

Abstract—Experiments, performed both in water and air, yielded natural convection heat transfer coefficients for cubes positioned in as many as 13 orientations in the gravity field. The orientation-related variations in the heat transfer were in the 10–12% range for water and in the 2–5% range for air. When represented in terms of the Nusselt and Rayleigh numbers, the water and air data differed by about 10%. The data were used to assess the prediction methods of King and of Lienhard. The former overpredicted the data by 40–58%, while the latter, although more accurate, underpredicted the data by as much as 23%. To correlate the data for the cube, the sphere, and the short vertical cylinder (height = diameter), all bodies of unity aspect ratio, a new characteristic length was formulated. The new length is based on the surface area of the body and on the square root of the area of the projection of the body on a horizontal plane. With the newly defined Nusselt and Rayleigh numbers and with an already established Prandtl number factor, the data were very tightly correlated. Flow visualization performed in water indicated that the flow was laminar and that there was no separation of the flow at the corners of the cube.

INTRODUCTION

THE PRESENT state of knowledge about natural convection heat transfer from three-dimensional bodies and complex two-dimensional bodies is highly incomplete. Even in the most recently published textbooks [1–3] and monographs [4], reference continues to be made to an unproven rule proposed by King [5] in 1932 for the evaluation of a characteristic length to be used in conjunction with a purportedly universal Nusselt–Rayleigh correlation. The correlation has long since been shown not to be universal and, very recently, the rule for the characteristic length was proven invalid for a body for which it was recommended by King, namely, a short vertical cylinder (height = diameter) [6]. An alternate proposal by Lienhard [7, 8] of a characteristic length and an accompanying Nusselt–Rayleigh correlation yielded better predictions for the short vertical cylinder of [6] than did the King procedure. There were, however, significant deviations between the predictions of the Lienhard method and the experimental data.

In addition to the short vertical cylinder, experimental results have been published for natural convection from spheres [9–11], oblate and prolate spheroids [12], and cylinders with hemispherical end caps [9]. In as-yet unpublished experiments [13], heat transfer results were obtained for a sphere, a vertically aligned bi-sphere, and a cube positioned in three symmetric orientations. The experiments of [13] were performed in air using a transient technique in which measurements were made of the temperature decay of a preheated solid.

The present investigation of external natural convection encompassed a many-faceted experimental study complemented by a major correlation effort. In recognition of the fact that a cube represents a variety of different bodies depending on its orientation in the gravity field, the cube was chosen as the object of the experimental work. As many as 13 different orientations were employed during the course of the experiments. The experimental work consisted of three parts: (1) heat transfer measurements in water ($Pr \sim 5.6$–6.7), (2) heat transfer experiments in air ($Pr \cong 0.71$), and (3) flow visualization in water.

The two different fluids were used not only to enlarge the range of the Rayleigh number but also to assess the dependence of the heat transfer results on the Prandtl number. Over all, the Rayleigh number (based on the cube side dimension) extended from 2300 to 10^7. Different apparatus were employed for the water and air experiments to accommodate the distinctive heat transfer characteristics of the two fluids. All the experiments were carried out under steady-state conditions and for the uniform wall temperature boundary condition.

The flow visualization was performed by observing the motion of laser-illuminated white plastic granules. The main focus of the visualization work was to identify the flow regime (laminar or turbulent) and to establish the behavior of the flow at the corners of the cube (separation or no separation).

The measured Nusselt numbers were employed to assess the accuracy of the predictions of the King and Lienhard methods that were discussed earlier. The insufficiencies of the predictions prompted a correlation effort aimed at accommodating all of the independent parameters (cube orientation, Rayleigh number, and Prandtl number). Based on the tightness of the resulting correlation of the cube data, the method was applied to the other bodies of unity aspect ratio for which data are presently available (i.e. the sphere and the short vertical cylinder). This yielded a tight correlation for all three bodies (and, presumably, for other bodies of unity aspect ratio) covering the Rayleigh number range from 200 to 1.5×10^9.

NOMENCLATURE

A	surface area of body
A_{horiz}	area of projection of body on horizontal plane
D	diameter of sphere or short vertical cylinder
D^{**}	equivalent diameter, equation (13)
$F(Pr)$	function of Prandtl number, equation (14)
g	acceleration of gravity
h	average heat transfer coefficient
k	thermal conductivity
L^*	characteristic length
L^{**}	characteristic length, equation (13)
Nu_S	Nusselt number based on S
Nu^*	Nusselt number based on L^*
Nu^{**}	Nusselt number based on L^{**}
Pr	Prandtl number
Q	convective heat transfer rate
Q_{rad}	radiative heat transfer rate
Ra_S	Rayleigh number based on S
Ra^*	Rayleigh number based on L^*
Ra^{**}	Rayleigh number based on L^{**}
S	length of side of cube
T_w	surface temperature
T_∞	ambient temperature
Z	vertical coordinates of cube corners, Fig. 2.

Greek symbols

β	coefficient of thermal expansion
ε	emissivity
θ	orientation angles, equation (1)
ν	kinematic viscosity.

EXPERIMENTAL APPARATUS

As already noted, different apparatus were used in the water and air experiments. The main components of each apparatus included: (1) an electrically heated cube instrumented with thermocouples, (2) a power supply and instrumentation for voltage measurements, (3) a suspension system which served to support the cube and adjust its orientation, and instrumentation for quantifying the orientation, and (4) the fluid environment in which the cube was situated. The general features of the apparatus will now be described, with additional details available in [14]. The features specific to the flow visualization experiments will be discussed later in conjunction with the experimental procedure for carrying out the visualization work.

The cubes for the water and air experiments were fabricated according to the same design, which is illustrated in Fig. 1 in a cross-sectional view cut through the middle of the cube. As seen there, the cube consisted of an outer shell, a wire-wound heater core, and inserted thermocouple-equipped plugs. The two cubes differed only in the material used for the outer shell, copper for the water experiments and aluminum for the air experiments. In view of the relatively high heat transfer coefficients for water, the use of copper was essential for the attainment of the uniform wall temperature boundary condition. In the air case, both copper and aluminum would have yielded temperature uniformity. Aluminum was chosen on the basis of radiation heat transfer considerations, since it can be polished to a more-enduring, low-emissivity surface finish than can copper. The surfaces of the copper cube were finished with very fine wet-or-dry sandpaper, while the surfaces of the aluminum cube were polished to a high luster with a succession of lapping compounds.

Both cubes were designed to have a side dimension (on the external surface) of 3.810 cm, with final dimensions, after surface finishing, very close to the design value. The outer shell, which had a uniform thickness of 0.635 cm, consisted of a main body which housed the heater core and a cap which closed the top of the cube assembly. The cap was fixed in place by nut-like fasteners, each situated in a recess at each of the four corners. Three of the fasteners also served as anchor points for nylon lines used to suspend the cube. The exposed face of each fastener was finished so as to present a hydrodynamically smooth surface to the flow, with a special low-emissivity finish for the fasteners used for the aluminum cube.

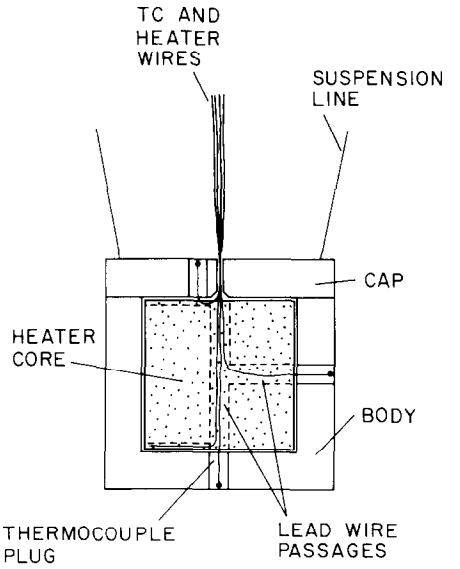

FIG. 1. Cross-sectional view of the cube.

Four precalibrated chromel–constantan thermocouples were installed in the walls of the cube, respectively at the centers of the top face, the bottom face, and a side face, and near a bottom corner. The thermocouples were made of 40-gauge, Teflon-coated wire. Their junctions were positioned about 0.013 cm from the exposed surface of the cube. This close approach to the surface was made possible by preinstalling each thermocouple in a short segment of 0.318-cm-diameter copper or aluminum rod and then pressing the segment into the cube wall to achieve an interference fit. The thermocouple lead wires were led out through passages in the heater core.

The heater core was a wire-wound block of aluminum that had been machined to fit into the cube body with minimal clearance. Aluminum was chosen as the core material to assist in the attainment of temperature uniformity and because it could be anodized to provide an electrically insulating layer for the prevention of short circuits. The heating wire, 0.013-cm chromel covered with Teflon insulation, was wound in 17 circumferential grooves and held in place by 0.002-cm-thick pressure-sensitive tape. As seen in Fig. 1, the lead wires for both the heater and the thermocouples emerged from a small hole centered in the cap of the cube.

Power was supplied to the heater by a D.C. source with a 0.01% voltage stability during steady-state operation (a different supply for the water and air experiments, to accommodate the different power levels). Not only did the use of D.C. provide better stability than is achievable from conventional regulated A.C. supplies, it also enabled more accurate voltage measurements than are possible with A.C. The heater and current shunt voltages were read to at least four significant figures, while the thermocouple emfs were read to 1 μV.

The cube was hung by three nylon lines from a rigid, immovable suspension brace. The brace was equipped with adjustable devices to provide precise control of the length of each nylon line and, thereby, to control the orientation of the cube. The adjustment devices were those used to tune guitar strings. They enabled length changes as small as 0.0013 cm to be made in the support lines. In various of the cube orientations, certain support lines had to exert a downward force rather than an upward force. The required change of direction was accomplished by the use of a pulley.

As will be elaborated shortly, the orientation of the cube is to be specified here in terms of two angles which were evaluated from measurements of the vertical elevations of three of the corners of the uppermost face. These elevation measurements were made with optical cathetometers having a resolving power of 0.005 cm.

The water experiments were performed utilizing a tank-in-tank arrangement. The water in the inner tank served as the fluid environment for the heated cube, while the water in the intertank space functioned as a buffer which thermally decoupled the fluid environment from the laboratory. A circulation pump was situated in the intertank space to stir the water and thereby prevent stratification. The effectiveness of the thermal decoupling was aided by insulation which sheathed the outside of the outer tank at all sides and at the bottom. A sheet of insulation lined with impermeable plastic served to cover the top of both tanks.

Both tanks were of plexiglass, with respective dimensions of $61 \times 61 \times 51$ cm and $81 \times 81 \times 56$ cm (length × width × depth). Distilled water was supplied to both the inner tank and the intertank space. A vertical array of four thermocouples equally spaced at 14-cm intervals was installed in the inner tank to measure the temperature of the water ambient for the cube.

The laboratory in which the air experiments were performed (dimensions $7.2 \times 4.6 \times 2.7$ m) was designed for thermal stability and isolation from external disturbances. The walls, ceiling, and floor of the laboratory are backed by 35 cm of cork, and there are no ducts, grilles, or vents through which air may pass into or out of it. It is located in a deep basement, away from external walls, and is buffered by a surrounding never-used room. Various high heat capacity objects situated within the laboratory add to its thermal stability. Furthermore, the power supply, digital voltmeter, and barometer were located in the surrounding room.

The ambient temperature was measured by an array of four thermocouples arranged vertically, with an inter-thermocouple spacing of 29 cm. Each thermocouple was shielded with multiple layers of aluminum foil to prevent its reading from being influenced by radiation from the cube.

EXPERIMENTAL PROCEDURE

The orientation of the cube in the gravity field was one of the key parameters of the research, and the establishment of the selected orientations was an important step in the experimental procedure. The scheme used to quantify the orientation is illustrated in Fig. 2. In the figure, the cube is shown in an arbitrary orientation, with the uppermost face shaded to delineate it from the other faces. The corner of the cube having the highest elevation is designated as point O, while the corners of the uppermost face that are connected to O along the edges of the face are denoted as A and B. The vertical coordinates of the aforementioned corners, relative to an arbitrary datum, are Z_O, Z_A, and Z_B. In terms of these coordinates, angles θ_1 and θ_2 will now be defined and subsequently used to characterize the orientation.

$$\theta_1 = \sin^{-1}[(Z_O - Z_A)/S],$$
$$\theta_2 = \sin^{-1}[(Z_O - Z_B)/S]. \quad (1)$$

The designation (θ_1, θ_2) will be utilized in describing the orientation of the cube. Thus, for example, the

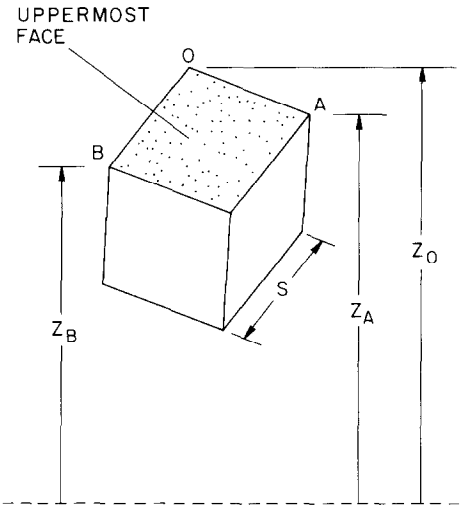

FIG. 2. Definition of the orientation of the cube.

standard horizontal top/horizontal bottom/vertical sides case is characterized by (0°, 0°). This is one of the three orientations which possess at least two vertical planes of symmetry. The second symmetric orientation, (45°, 0°), may be arrived at from the (0°, 0°) case by a 45° rotation about one of the horizontal edges. This orientation will henceforth be referred to as edge-over-edge, since the uppermost and lowermost horizontal edges lie in a common vertical plane. In the third symmetric orientation, the most streamlined, the uppermost and lowermost corners lie on the same vertical line. This case, to be termed corner-over-corner, is characterized by (35.3°, 35.3°) (note that $\sin^{-1}(1/\sqrt{3}) = 35.3°$).

The establishment of a preselected cube orientation was accomplished by setting the elevation differences $(Z_O - Z_A)$ and $(Z_O - Z_B)$, which required a trial and error process. After each tentative adjustment of the support lines, a measurement of the elevations was made using the cathetometers, and these operations were continued (normally 10–15 cycles) until the desired orientation was attained. The elevations were checked periodically during a fixed-orientation sequence of data runs.

A prerequisite for the initiation of a data run was the absence of stratification. For the air experiments, stratification was altogether absent except after the laboratory had been entered. Such post-entry stratification decayed well before the elapse of the 12-h, between-run interval that was allowed in the work with air.

For the water experiments, stirring of the water was employed to ensure the absence of stratification. It was found from auxiliary experiments that a time lapse of 1 h was more than sufficient for the decay of the stirring-induced disturbances, after which a data run was initiated by energizing the cube heating element. Steady-state heat transfer conditions were attained within several minutes after the initiation of the run. The water in the tank was not stirred between successive data runs unless the stratification exceeded 1% of the cube-to-ambient temperature difference.

Flow visualization

The flow visualization work was performed in water. White plastic granules (Goodyear Pliolite VT resin) with a specific gravity of 1.026 and a 20–50 μm size range were used to track the convection patterns. The particles were able to remain suspended in the water for approximately three days. A 5 mW helium–neon laser with a simple convex cylindrical lens provided a narrow plane of light to illuminate a cross section of the flow field. To enhance the relative brightness of the tracer particles passing through the illuminated plane, provisions were made to achieve a dark background. Furthermore, a mirror assembly was positioned behind the cube to reflect light into the cube shadow. The particle motion was photographed on black and white ISO 400 film with a 35 mm camera having a 50 mm f/1.4 lens.

The experimental procedure for the flow visualizations involved preparatory steps similar to those for the heat transfer data runs plus additional measures related to the alignment of the cube and the quiescence of the water environment. In particular, precise alignment was necessary to ensure that a preselected face of the cube was situated at the intersection of the vertical focal planes of the laser and the camera. Furthermore, since the flow patterns were found to be quite sensitive to extraneous motions in the water, temporary baffle plates plus a longer settling time were both used to ensure the decay of the stirring-induced disturbances. During the settling period, the particle population was adjusted and the optical system aligned.

The flow visualization runs were carried out at the highest Rayleigh number of the present investigation. Once steady-state heat transfer conditions had been attained, photography was initiated, with exposure times ranging from 10 s to 8 min.

DATA REDUCTION

The average heat transfer coefficient for the cube was evaluated from the defining equation

$$h = Q/A(T_w - T_\infty). \tag{2}$$

For the water experiments, the heat transfer rate Q was obtained directly from the power input to the cube heater, while for the air experiments, a subtractive correction was applied to account for the radiative heat loss Q_{rad}. To facilitate the calculation of the radiative loss, the emissivity ε of the cube surface was measured at 25 and 100°C with a Gier–Dunkle reflectometer, giving $\varepsilon = 0.032$ and 0.038. The ε values at other temperatures were obtained by linear interpolation and extrapolation. Then, Q_{rad} was evaluated from

$$Q_{rad} = \varepsilon\sigma A(T_w^4 - T_\infty^4). \tag{3}$$

In both equations (2) and (3), A denotes the surface area of the cube.

The cube surface temperature T_w which appears in equations (2) and (3) was determined by averaging the readings of the four thermocouples embedded in the cube wall. Deviations from the average were typically about 1.5% of $(T_w - T_\infty)$ in the water experiments and about 0.25% of $(T_w - T_\infty)$ in the air experiments. The temperature T_∞ was also obtained as an average, based on the readings of the three ambient thermocouples closest to the cube (deviations from the average were well under 1%). Note that for the Q_{rad} calculations, it was assumed that the temperature of the laboratory contents and of the bounding walls was equal to T_∞.

If L^* represents a characteristic dimension of the cube, the heat transfer coefficient can be expressed in dimensionless form by the Nusselt number Nu^*

$$Nu^* = hL^*/k. \tag{4}$$

The other dimensionless groups of the problem are the Prandtl and Rayleigh numbers. With the L^* characteristic dimension, the Rayleigh number is

$$Ra^* = [g\beta(T_w - T_\infty)L^{*3}/\nu^2]Pr \tag{5}$$

and $Pr = c_p\mu/k$. The thermophysical properties appearing in Nu, Ra and Pr were evaluated at the film temperature $\frac{1}{2}(T_w + T_\infty)$, except that $\beta = 1/T_\infty$ for the air data. During the presentation of results which follows, the characteristic length L^* will be evaluated in several ways as the data are interpreted from different points of view.

RESULTS AND DISCUSSION

In the first sections of the presentation, the data will be treated as a whole (i.e. all orientations, Rayleigh numbers, and fluids) and compared with those for other bodies of unity aspect ratio, applied to test the King and Lienhard prediction methods, and used as the basis of a correlation effort. Then, the effects of orientation on the cube heat transfer characteristics will be examined in detail. The presentation will conclude with a report of the findings of the flow visualization.

Nusselt numbers

Attention will first be turned to Fig. 3(a), where the cube heat transfer data are plotted in terms of Nusselt and Rayleigh numbers based on the side S as the characteristic dimension, i.e.

$$L^* = S. \tag{6}$$

The data for $Ra_S < 3 \times 10^5$ correspond to the experiments performed in air, while those for $Ra_S > 3 \times 10^5$ are from the water experiments. Data for all of the investigated cube orientations have been plotted in the figure, but many of the points are obscured by the overlap of the symbols. All of the data will be displayed later when the effects of orientation are examined in greater detail.

In addition to the cube data, Fig. 3(a) includes lines which represent the Nusselt numbers for the other three-dimensional bodies of unity aspect ratio for which results are available, namely, the short vertical cylinder [6] (height = diameter) and the sphere [10, 11]. For both of these cases, the diameter D was used as the characteristic dimension in Nu and Ra. The sphere data are seen to lie somewhat higher than those for the cube, with the greatest deviations (20–25%) at the lowest Rayleigh numbers. On the other hand, the data for the short cylinder and the cube are virtually coincident.

The spread exhibited by the cube heat transfer data is not scatter. Rather, it reflects the response of the heat transfer to changes in orientation. At any given Rayleigh number, the orientation-induced spread of the data is bounded below by the standard horizontal

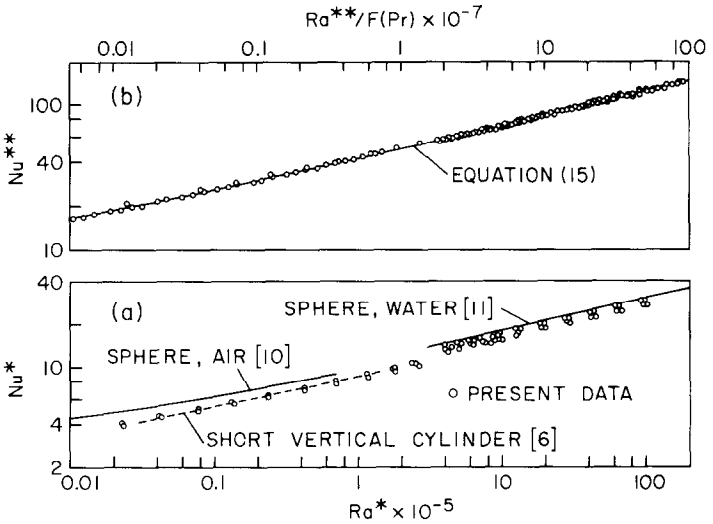

FIG. 3. Nusselt number results: (a) based on $L^* = S$ for the cube and $L^* = D$ for the sphere and short vertical cylinder; (b) based on L^{**} of equation (13).

top/horizontal bottom/vertical sides case (0°, 0°) and above by the corner-over-corner case (35.3°, 35.3°). Since the former corresponds to a blunt body and the latter to a more streamlined configuration, it can be concluded that there is a trend toward higher heat transfer coefficients with greater streamlining.

It is seen that the spread of the water data is greater than that for the air data (10–12% compared with 2–5%), indicating a greater responsiveness to orientation for the former. Note also that a logical extrapolation of the air data to the Rayleigh number range of the water data (and vice versa) suggests a Prandtl-number-related spread on the order of 10%. A similar finding is suggested by the air and water data for the sphere. Thus, the inclusion of the Prandtl number in the Rayleigh number does not completely eliminate the effect of the Prandtl number for these three-dimensional geometries.

The algebraic description of the data will be dealt with later in depth, both from the standpoint of a universal correlation and of the individual orientations of the cube. Here, the most straightforward representation of the data of Fig. 3(a) will be employed, namely, a power law of the form $Nu = CRa^n$. If Nu_S and Ra_S denote the Nusselt and Rayleigh numbers based on the side dimension S, the respective least-squares correlations for the air and water data are

$$Nu_S = 0.786 Ra_S^{0.207}, \quad Pr \cong 0.7 \tag{7}$$

$$Nu_S = 0.601 Ra_S^{0.239}, \quad Pr \cong 6 \tag{8}$$

with data spreads of ±3.5 and ±7% respectively.

Comparisons with predictive methods

The cube data will now be used to test the predictions of the widely quoted King method [5]. The first step is to evaluate the characteristic dimension L^* according to King's rule

$$1/L^*_{\mathrm{King}} = 1/L_H + 1/L_V \tag{9}$$

where L_H and L_V are, respectively, the horizontal and vertical dimensions of the body. There is some uncertainty about how to interpret L_H and L_V for cube orientations other than the standard horizontal top/horizontal bottom/vertical sides case (0°, 0°), for which $L_H = L_V = S$ and

$$L^*_{\mathrm{King}} = S/2. \tag{10}$$

For this reason, only the data for the (0°, 0°) orientation will be used in the assessment of the King method.

Those data have been rephrased according to equation (10) and plotted in Fig. 4(a). Also appearing in the figure is King's Nusselt–Rayleigh correlation, which, together with the L^* rule of equation (9), is supposed to predict the natural convection heat transfer characteristics of arbitrary bodies. The figure also includes lines representing the results for the sphere and short vertical cylinder, also rephrased using L^* from equation (9).

Examination of Fig. 4(a) shows that King's method overpredicts the cube data by 40–58%, depending on the Rayleigh number. It also substantially overpredicts the sphere and cylinder results. These findings provide a strong argument against the continued reference to King's method in textbooks and monographs.

The cube data will next be used to test the Lienhard prediction method [7, 8]. Lienhard recommended the use of a characteristic length L^* equal to the length of travel of fluid in the boundary layer. Even for the (0°, 0°) orientation, numerous paths of travel may be envisioned, yielding a range of L^* from $2S$ to $(1+\sqrt{2})S$.

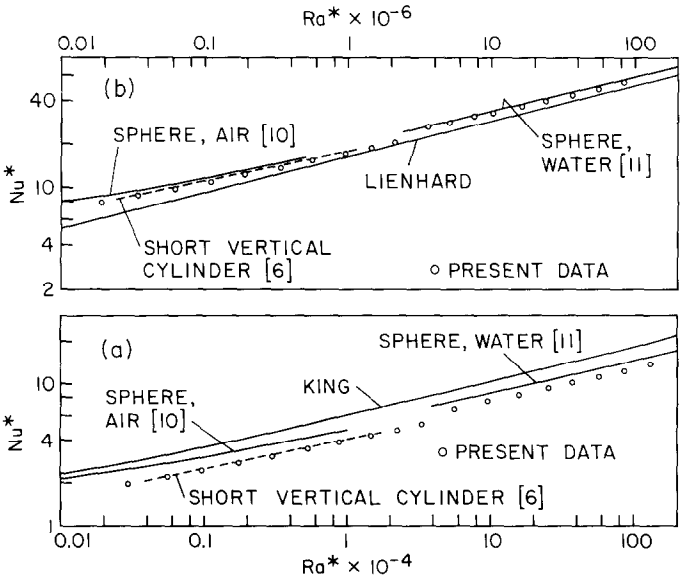

FIG. 4. Comparison of experimental results with prediction methods: (a) King's method; (b) Lienhard's method.

The other orientations offer even a greater range of possibilities for L^*.

The data for the (0°, 0°) case will be used for comparison with the Lienhard predictions along with the choice (the shortest path)

$$L^*_{\text{Lien}} = 2S \tag{11}$$

which shows the Lienhard method in its best light. In conjunction with the L^* value, Lienhard recommends the Nusselt–Rayleigh relation

$$Nu = 0.52Ra^{1/4}. \tag{12}$$

The rephrased Nu, Ra data for the (0°, 0°) orientation are plotted in Fig. 4(b) along with equation (12). The figure also includes the property rephrased results for the sphere and the short horizontal cylinder.

As seen in the figure, the Lienhard method underpredicts the data, in contrast to the overpredictions of the data by the King method. The air data for the cube are underpredicted by 4–23%, while the water data are underpredicted by 8–15%. The underpredictions for the sphere and the short cylinder are somewhat greater than those for the cube.

The Lienhard method provides more accurate predictions of the cube data than does the King method but is still of marginal utility. Furthermore, the interpretation of the characteristic length is uncertain for bodies with alternative paths of travel in the boundary layer.

Universal correlation

The insufficiencies of the King and Lienhard methods provided the motivation for the development of a correlation which would represent the cube data to high accuracy over the entire investigated range of orientations, Rayleigh numbers, and Prandtl numbers. A second objective of the correlation effort was to bring together the data for the cube with those for other bodies of unity aspect ratio.

The key to the correlation is the definition of the characteristic length, which will be denoted by L^{**} to set it apart from prior definitions

$$L^{**} = A/D^{**}, \quad \pi(D^{**})^2/4 = A_{\text{horiz}}. \tag{13}$$

In this equation, A is the surface area of the body [as in equations (2) and (3)], while A_{horiz} is the area of the projection of the body on a horizontal plane situated either above or below the body. The quantity D^{**} is an equivalent diameter based on A_{horiz}. For example, for the (0°, 0°) orientation of the cube, $D^{**} = 2S/\sqrt{\pi}$ and $L^{**} = 3S\sqrt{\pi}$. The Nusselt and Rayleigh numbers based on L^{**} will be respectively denoted by Nu^{**} and Ra^{**}.

To account for the Prandtl number effect, functions $F(Pr)$ were examined which had been used successfully in correlating heat transfer data for other problems over a wide range of Prandtl numbers. It was found that the function [15]

$$F(Pr) = [1 + (0.492/Pr)^{9/16}]^{16/9} \tag{14}$$

was highly effective in correlating the air and water data for the cube.

The cube data for all of the investigated orientations are plotted as Nu^{**} vs $Ra^{**}/F(Pr)$ in Fig. 3(b). It is evident that the congruence attained by the data due to the new characteristic length is excellent, and that the air and water data are continuous owing to $F(Pr)$. The data distribution has a slight curvature, with a tendency for the slope to decrease at lower Ra^{**}. This trend is consistent with the literature and reflects the thickening of the boundary layer with decreasing Rayleigh number.

The data were fitted with the equation

$$Nu^{**} = 6.65 + 0.623[Ra^{**}/F(Pr)]^{0.261} \tag{15}$$

which is also plotted in Fig. 3(b). It is noteworthy that 78% of the data fall within 2% of the correlating equation and that the maximum deviation is only 5.5%. Note that equation (15) accommodates all of the orientations of the cube.

Although the constant 6.65 was determined empirically, it may be regarded as the limiting value of Nu^{**} as $Ra^{**} \to 0$. The pure conduction limit ($Ra^{**} = 0$) was calculated [16] to be $Nu_S = 1.383$. Since L^{**}/S ranges from 5.317 for the (0°, 0°) orientation to 4.040 for the (35.3°, 35.3°) orientation, the conduction limit for Nu^{**} ranges from 5.587 to 7.353, which brackets the empirical value of 6.65.

The success of the Nu^{**} and $Ra^{**}/F(Pr)$ groups in correlating the cube data prompted their use for other bodies of unity aspect ratio. The available experimental results for the sphere in air [10, 13], sphere in water [11], short vertical cylinder in air [6], and cube in air [13], as well as the present air and water data for the cube, have all been rephrased in terms of Nu^{**} and $Ra^{**}/F(Pr)$ and correlated by the equation

$$Nu^{**} = 5.748 + 0.752[Ra^{**}/F(Pr)]^{0.252} \tag{16}$$

where 84% of the data fall within 5% of the correlation, and the maximum deviation is 9.5%. The data on which equation (16) is based extend over the Rayleigh number range from about 200 to 1.5×10^9. Note that the empirical constant 5.748 and the conduction limit for the sphere, $Nu^{**} = 6.283$, fall within the aforementioned range of conduction limits for the cube.

Considering that equation (16) is based on data from four different sources and encompasses a variety of geometries, the tightness of the correlation is remarkable. It is believed that equation (16) can be applied with confidence for moderate extensions of Ra^{**} beyond the range from 200 to 1.5×10^9, for bodies having aspect ratios which deviate slightly from unity, and for all Prandtl numbers (except, perhaps, for liquid metals). However, the correlation is not recommended for bodies whose aspect ratios deviate significantly from unity (Table 4.3 of [14]).

Effect of cube orientation

A detailed examination will now be made of the effect of cube orientation on the heat transfer characteristics.

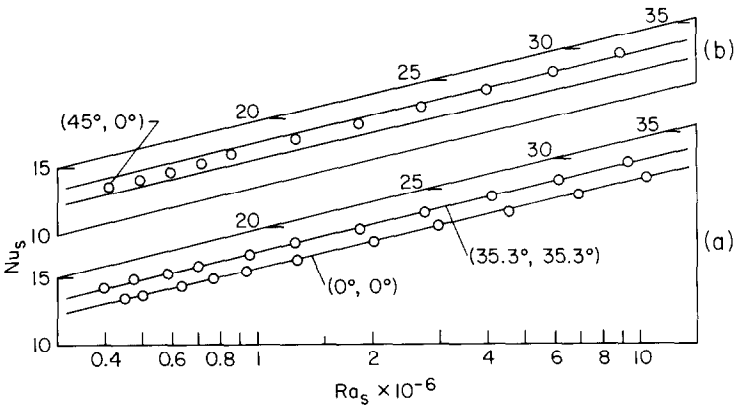

FIG. 5. Nusselt numbers for the three symmetric orientations (water experiments).

For this purpose, the data will be presented in terms of Nu_S and Ra_S rather than Nu^{**} and Ra^{**}. This choice was prompted by the fact that S is common to all orientations, so that variations of Nu_S with orientation are direct reflections of the variations of the heat transfer coefficient. As noted earlier in connection with Fig. 3(a), the water data were found to be more sensitive to orientation than the air data. Correspondingly, the number of cube orientations examined during the course of the water experiments was greater than for the air experiments, specifically, 13 vs 4. The presentation will begin with the data for water.

Figure 5 displays the Nusselt number results for the three symmetric orientations (0°, 0°), (35.3°, 35.3°), and (45°, 0°). As was pointed out earlier, the Nu_S, Ra_S distributions for the first two of these are, respectively, the lower and upper bounds for the Nusselt numbers of all the other orientations. These cases will, therefore, be regarded as baselines. They are displayed in Fig. 5(a), where the solid lines are least-squares, power-law representations whose equations are

$$Nu_S = 0.690 Ra_S^{0.226}, \quad (0°, 0°) \tag{17}$$

$$Nu_S = 0.717 Ra_S^{0.231}, \quad (35.3°, 35.3°). \tag{18}$$

The least-squares lines are seen to be excellent representations of the data. They are virtually parallel, with the upper line lying 10–12% above the lower line. The spread constitutes the extent of the orientation effect for the water experiments.

The Nusselt number data for the third symmetric case, (45°, 0°), are plotted in Fig. 5(b), where they are compared with the least-squares representations of the baseline cases. It is seen that the (45°, 0°) data tend to favor the lower baseline at smaller Rayleigh numbers and the upper baseline at larger Rayleigh numbers. This trend will be rationalized shortly.

In Fig. 6, Nusselt number results are presented for orientations characterized by $\theta_1 > 0$ and $\theta_2 = 0$ (i.e. a single angle of tilt). These orientations may be arrived at from the (0°, 0°) case by a rotation of θ_1 about one of the horizontal edges. To avoid data overlap, the figure is subdivided into (a), (b), and (c) parts. In each part of the figure, results for one or more $(\theta_1, 0°)$ cases are plotted along with the least-squares representations of the baseline cases.

For small θ_1, (2.5 and 5°), the data cling to the lower baseline over most of the Rayleigh number range and lift off slightly at the upper end of the range. At the larger θ_1, (15 and 45°), the data continue to favor the lower

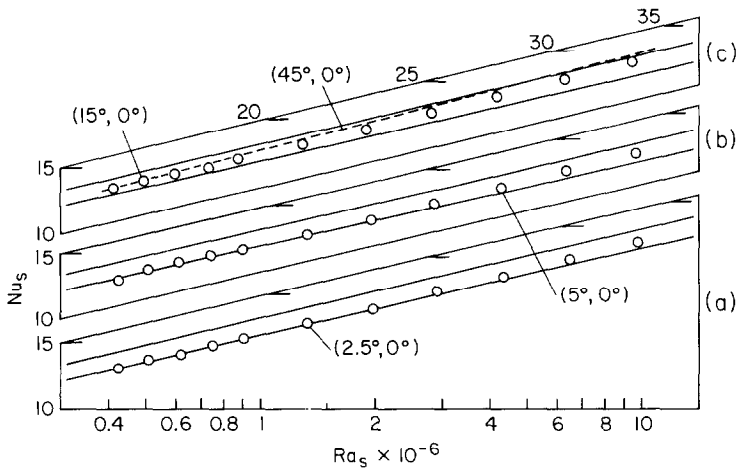

FIG. 6. Nusselt numbers for orientations having a single non-zero angle of tilt (water experiments).

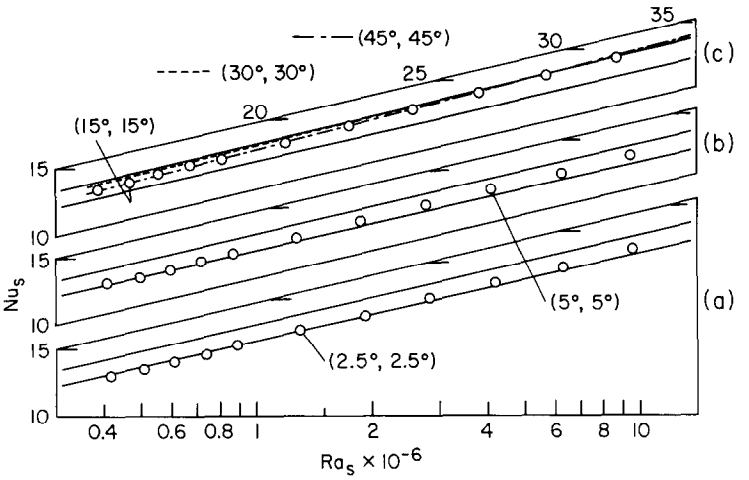

FIG. 7. Nusselt numbers for orientations having equal values of the two tilt angles (water experiments).

baseline at the smaller Ra_S but approach the upper baseline at larger Ra_S.

In rationalizing the tendency of the data to favor one or the other baseline as the Rayleigh number is varied, it is useful to recall the conclusion, drawn from Fig. 3(a), that more streamlined cube orientations yield higher heat transfer coefficients. Furthermore, for a given cube orientation, Rayleigh-number-related changes in the flow pattern may affect the apparent degree of streamlining of the cube. In particular, if the stagnation point were to shift from the center of a downfacing facet to a position nearer to the low point of the facet, the cube would appear to be more streamlined. It is conjectured that such a shift does occur with increasing Rayleigh number, causing a heightened increase of the Nusselt number.

The next set of orientations to be examined are characterized by common values of θ_1 and θ_2. These results are plotted in Figs. 7(a), (b) and (c), where, again, the baselines are included for reference. Note that the baseline cases (0°, 0°) and (35.3°, 35.3°) are also characterized by $\theta_1 = \theta_2$. It is seen that the Nusselt number increases as the angles increase from 0°, but the increase is not monotonic in the lower and intermediate portions of the Rayleigh number range, where a maximum occurs when $\theta_1 = \theta_2 = 35.3°$. At the upper end of the range, the increase appears to be monotonic, but the results for $\theta_1 = \theta_2 = 15, 30$ and 45° are virtually identical.

The final figure dealing with the water data is Fig. 8, where all of the displayed orientations are characterized by θ_1 and θ_2 values equal to 15° and larger. The main message of this figure is that the Nusselt numbers for this range of angles are all very close to the upper baseline.

Attention will next be turned to the orientation effects for the air data, and Fig. 9 has been prepared for this purpose. Figure 9(a) displays the data and fitted lines for the baseline cases, (0°, 0°) and (35.3°, 35.3°). The fitted lines are

$$Nu_S = 1.20 + 0.387 Ra_S^{0.262}, \quad (0°, 0°) \qquad (19)$$

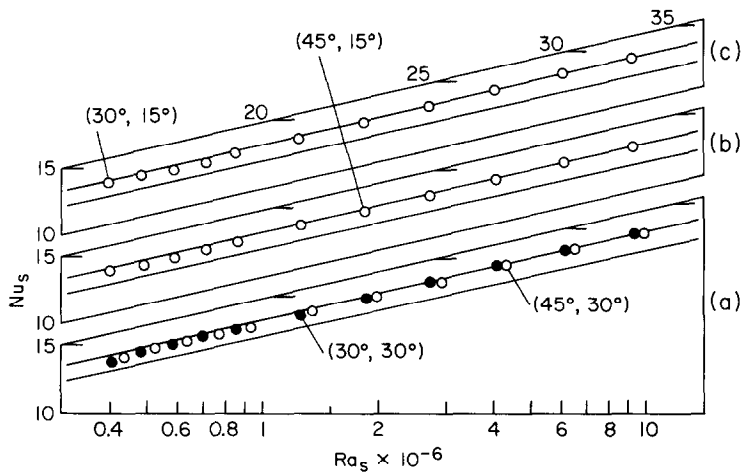

FIG. 8. Nusselt numbers for orientations having intermediate and large tilt angles (water experiments).

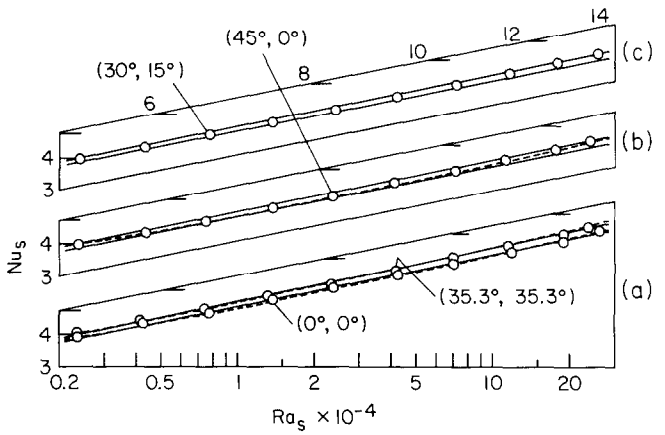

FIG. 9. Nusselt numbers for various orientations (air experiments).

$$Nu_S = 1.41 + 0.338 Ra_S^{0.267}, \quad (35.3°, 35.3°). \quad (20)$$

The spread between the two baseline cases is only 2–5%, which constitutes the extent of the orientation effect for the air data. This minimal spread is affirmed by the data of [13], which are depicted by dashed lines in Fig. 9(a). The agreement of the present data and that of [13] is near-perfect. Figures 9 (b) and (c) convey data for the (45°, 0°) and (30°, 15°) orientations and include the baselines for reference purposes. The data for these orientations are bounded between the baselines. The (b) part of the figure further confirms the excellent agreement between the present data and [13].

Flow visualization results

The visualization work was performed for the (0°, 0°) and (45°, 0°) cases, respectively representing blunt and streamlined orientations of the cube (the most streamlined case, (35.3°, 35.3°), was not well suited to the visualization technique). The visualization experiments were carried out in water at the high end of the Rayleigh number range ($Ra_S \sim 10^7$) in order to attain the most vigorous possible flow and, thereby, to enhance the sharpness of the streak pattern.

Despite all of the care and precautions that were taken, none of the numerous photographs was judged to possess the sharpness needed for journal reproduction and publication. Nevertheless, the visualization work did produce definitive and significant findings as follows: (1) there was no evidence of flow separation and recirculation at any of the corners of the cube and (2) the flow was laminar. On this basis, it can be expected that laminar, non-separating flow will prevail for all $Ra_S \leqslant 10^7$ in water. In the absence of other information, this conclusion may be extended to air, but with caution.

CONCLUDING REMARKS

The experiments performed here have provided definitive information on the response of the cube heat transfer to orientation and have yielded data of high accuracy suitable for testing prediction methods and for serving as the basis of a correlation effort. As many as 13 different orientations of the cube in the gravity field were investigated during the experiments. Both water and air were used as the fluid environment of the cube in order to assess the effect of Prandtl number on the heat transfer. The heat transfer experiments were supplemented by flow visualization studies in water, wherein white plastic granules tracked the convective motions.

The cube heat transfer was more sensitive to orientation in water than in air. The lowest heat transfer was associated with the standard horizontal top/horizontal bottom/vertical sides case, while the highest heat transfer was provided by the more streamlined corner-over-corner orientation. Over all, the orientation-related variations in heat transfer were in the 10–12% range for water and in the 2–5% range for air.

When represented in terms of the Nusselt and Rayleigh numbers, the heat transfer data for water and air differed by about 10%.

The cube data were used to assess the accuracy of the prediction methods of King and of Lienhard. Each method consists of a rule for evaluating the characteristic length of the body and a Nusselt–Rayleigh relation. The King method overpredicted the data by 40–58%, a finding which argues against its continued citation in textbooks and monographs. The predictions of the Lienhard method were more accurate, but underpredictions of the data as large as 23% were encountered.

The insufficiencies of the King and Lienhard methods motivated a major correlation effort. A new characteristic length L^{**} was evolved which is based on the surface area of the body and on the square root of the area of the projection of the body on a horizontal plane situated either above or below the body. The Prandtl number effect was accommodated by a function $F(Pr)$ which had been used previously in the literature to correlate heat transfer data over a wide range of Prandtl numbers. When represented in terms

of Nu^{**} and $Ra^{**}/F(Pr)$, the cube data for all orientations and for both water and air were correlated by equation (15) such that 78% of the data fell within 2% of the correlation.

The Nu^{**} and $Ra^{**}/F(Pr)$ correlation groups were then employed to bring together the heat transfer results for the three bodies of unity aspect ratio for which data are available, namely, the cube, the sphere, and the short vertical cylinder (height = diameter). The resulting correlation, equation (16), was again very tight, with 84% of the data falling within 5% of the equation.

The flow visualizations, performed in water and at the highest investigated Rayleigh number ($\sim 10^7$), indicated that the flow was laminar and that there was no separation of the flow at the corners of the cube.

REFERENCES

1. L. C. Burmeister, *Convective Heat Transfer*, p. 552. Wiley, New York (1983).
2. F. M. White, *Heat Transfer*, p. 347. Addison-Wesley, Reading, Mass. (1984).
3. H. Wolf, *Heat Transfer*, pp. 222–223. Harper and Row, New York (1983).
4. A. D. Kraus and A. Bar-Cohen, *Thermal Analysis and Control of Electronic Equipment*, p. 141. Hemisphere, Washington, D.C. (1983).
5. W. J. King, The basic laws and data of heat transmission—III. Free convection, *Mech. Engng* **54**, 347–353 (1932).
6. E. M. Sparrow and M. A. Ansari, A refutation of King's rule for multi-dimensional external natural convection, *Int. J. Heat Mass Transfer* **26**, 1357–1364 (1983).
7. J. H. Lienhard, On the commonality of equations for natural convection from immersed bodies, *Int. J. Heat Mass Transfer* **16**, 2121–2123 (1973).
8. J. H. Lienhard, *A Heat Transfer Textbook*, pp. 361–362. Prentice-Hall, Englewood Cliffs, New Jersey (1981).
9. W. Elenbaas, The dissipation of heat by free convection—horizontal and vertical cylinders; spheres, *Physica* **9**, 665–672 (1942).
10. T. Yuge, Experiments on heat transfer from spheres including combined natural and forced convection, *J. Heat Transfer* **82**, 214–220 (1960).
11. W. S. Amato and C. Tien, Free convection heat transfer from isothermal spheres in water, *Int. J. Heat Mass Transfer* **15**, 327–339 (1972).
12. G. D. Raithby, A. Pollard, K. T. G. Hollands, and M. M. Yovanovich, Free convection heat transfer from spheroids, *J. Heat Transfer* **98**, 452–458 (1976).
13. M. J. Chamberlain, Free convection heat transfer from a sphere, cube, and vertically aligned bi-sphere, M.A. Sc. thesis, University of Waterloo, Waterloo, Ontario (1983).
14. A. J. Stretton, Natural convection for a cube in various orientations, M.S. thesis, University of Minnesota, Minneapolis (1984).
15. S. W. Churchill and H. H. S. Chu, Correlating equations for laminar and turbulent free convection from a vertical plate, *Int. J. Heat Mass Transfer* **18**, 1323–1329 (1975).
16. M. M. Yovanovich, *Advanced Heat Conduction*. Hemisphere, Washington, D.C. (1984).

CONVECTION NATURELLE AUTOUR DE CUBES A ORIENTATION VARIABLE ET AUTOUR D'AUTRES CORPS A RAPPORT DE FORME UNITE

Résumé—Des expériences dans l'eau ou l'air, concernent les coefficients de convection naturelle pour des cubes positionnés selon treize orientations dans le champ de pesanteur. Les variations de coefficient liées à l'orientation sont dans le domaine 10–12 pour cent avec l'eau et 2–5 pour cent pour l'air. Représentés en termes de nombres de Nusselt et de Raleigh, les données pour l'eau et l'air diffèrent de dix pour cent environ. Les données sont utilisées pour vérifier les prédictions de King et de Lienhard. La première surestime les données de 40 à 58 pour cent, tandis que la dernière, bein que plus précise, sous-estime jusqu'à 23 pour cent. Pour unifier les résultats du cube, de la sphère, et d'un cylindre vertical court (hauteur = diamètre), tous les corps ayant un facteur de forme unité, on formule une nouvelle longueur caractéristique. Celle-ci est basée sur la surface du corps et sur la racine carrée de l'aire de projection du corps sur un plan horizontal. Les résultats sont très bien unifiés avec les nouveaux nombres de Nusselt et de Rayleigh et avec un facteur établi sur le nombre de Prandtl. Une visualisation de l'écoulement dans l'eau indique que l'écoulement est laminaire et qu'il n'y a pas de séparation aux coins du cube.

NATÜRLICHE KONVEKTION AN UNTERSCHIEDLICH ORIENTIERTEN WÜRFELN UND ANDEREN KÖRPERN MIT DEM SEITENVERHÄLTNIS EINS

Zusammenfassung—Zur Bestimmung des Wärmeübergangskoeffizienten bei natürlicher Konvektion an Würfeln wurden in mehr als 13 Orientierungen bezüglich der Schwerkraft Untersuchungen in Wasser und Luft durchgeführt. Abhängig von der Orientierung änderte sich der Wärmeübergang bei Wasser im Bereich 10–12% und bei Luft im Bereich 2–5%. In Form von Nusselt- und Rayleigh-Zahlen differierten die Ergebnisse der Untersuchungen mit Wasser um 10% von denen mit Luft. Die Ergebnisse wurden zur Bewertung der Berechnungsmethoden von King und Lienhard benutzt. Die erstere Methode liefert Ergebnisse, die um 40 bis 58% zu groß sind, während die letztere zwar genauer ist, aber die Ergebnisse um ganze 23% zu klein vorausberechnet. Um die Ergebnisse für den Würfel, die Kugel und den kurzen vertikalen Zylinder (Höhe = Durchmesser), alles Körper mit dem Seitenverhältnis eins, zu korrelieren, wurde eine neue charakteristische Länge eingeführt. Die neue Länge wird mit der Körperoberfläche und der Quadratwurzel der Körperprojektionsfläche auf eine horizontale Ebene gebildet. Mit den neu definierten Nusselt- und Rayleigh-Zahlen und einem bereits eingeführten Prandtl-Zahl-Faktor ließen sich die Ergebnisse sehr gut korrelieren. Die Sichtbarmachung der Strömung in Wasser zeigte, daß die Strömung laminar war und keine Strömungsablösung an den Würfelecken auftrat.

ЕСТЕСТВЕННАЯ КОНВЕКЦИЯ ВОКРУГ КУБОВ С РАЗЛИЧНОЙ ОРИЕНТАЦИЕЙ И ОТ ДРУГИХ ТЕЛ, ИМЕЮЩИХ ОТНОШЕНИЕ СТОРОН, РАВНОЕ ЕДИНИЦЕ

Аннотация—В результате экспериментов, проведенных как с водой, так и с воздухом, получены коэффициенты естественноконвективной теплоотдачи для кубов, находящихся в 13 различных положениях в гравитационном поле. Отличие от теплообмена в зависимости от ориентации составило для воды 10–12%, для воздуха 2–5%. Результаты для воды и воздуха, выраженные через числа Нуссельта и Рэлея, отличались приблизительно на 10%. Полученные данные использовались для оценки методов расчета Кинга и Линхарда. По Кингу результаты расчета завышались на 40–58%, в то время как по Линхарду, несмотря на повышенную точность, результаты занижались на 23%. Для обобщения данных по кубу, сфере и короткому вертикальному цилиндру (высота равна диаметру)—все тела имеют отношение сторон, равное единице,—введена новая характерная длина. Новая длина основана на площади поверхности тела и корне квадратном из площади проекции тела на горизонтальную плоскость. С помощью переопределенных чисел Нуссельта и Рэлея и числа Прандтля достигалась хорошая корреляция полученных данных. Визуализация течения для воды показала, что течение было ламинарным и отсутствовало его расслоение в углах куба.